CHAPTER 4

Computational Investigation on the p53(TAD1)-MDM2(NTD) Interaction Using the Potential of Mean Force Study

Computational Investigation on the p53(TAD1)-MDM2(NTD) Interaction Using the Potential of Mean Force Study

4.1. Abstract:

MDM2 proteins are found to be overproduced by many human tumors in order to inhibit the functioning of p53 molecules, a tumor suppressor protein. Thus, reactivating p53 functioning in cancer cells by disrupting p53-MDM2 interactions may offer a significant approach in cancer treatment. However, the structural characterization of the p53-MDM2 complex at the atomistic level and the mechanism of binding/unbinding of the p53-MDM2 complex still remain unclear. Therefore, we demonstrate here the probable binding (unbinding) pathway of TAD1 of p53 during the formation (dissociation) of the p53-MDM2 complex in terms of free energy as a function of reaction coordinate from the PMF study using two different force fields: ff99SB and ff99SB-ILDN. From the PMF plot, we noticed the PMF to have a minimum value at a p53-MDM2 separation of 12 Å, with a dissociation energy of 30 kcal mol^{-1}. We also analyzed the conformational dynamics and stability of p53 as a function of its distance of separation from MDM2. The secondary structure content (helix and turns) in p53 was found to vary with its distance of separation from MDM2. The p53-MDM2 complex structure with lowest potential energy was isolated from the ensemble at the reaction co-ordinate corresponding to the minimum PMF value and subjected to molecular dynamics (MD) simulation to identify the interface surface area, interacting residues at the interface and the stability of the complex. The simulation results highlights the importance of hydrogen bonds and the salt bridge between Lys94 of MDM2 and Glu17 of p53 in the stability of the p53-MDM2 complex. We also carried out the BFE calculations and the PRED analyses of the interface residues of the p53-MDM2 complex. We found the binding affinity between MDM2 and p53 is indeed high ($\Delta G_{bind}/\Delta G_{binding}$ = -7.29 kcal mol^{-1} from MM-PBSA and $\Delta G_{bind}/\Delta G_{binding}$ = -53.29 kcal mol^{-1} from MM-GBSA). The total binding energy obtained using MM-PBSA method was noticed to be closer to the experimental values (-6.4 to -9.0 kcal mol^{-1}). The p53-MDM2 complex binding profile was observed to follow the same trend even in the duplicate simulation run and also in the simulation carried out with different force field. We found Lys51, Leu54, Tyr100, and Tyr104 from MDM2 and the residues Phe19, Trp23, and Leu26 from p53 provide the highest energy contributions for

the p53-MDM2 interaction.

4.2. Introduction:

Protein-Protein interactions have a dominant role in the identification of huge number of biological processes as well as biomolecules [495-497]. Most of the essential biological processes such as enzyme catalysis, immune system modulation, gene expression, and adjustment of signal pathways depend crucially on the regulation of the protein-protein interactions [498-500]. Moreover, the designing of drugs is mainly based on the modification of protein-protein interactions. The current focus of the researchers is on studying the structure and function of proteins. This is because the root cause of many diseases are related to disorders present in proteins.

The tumor suppressor p53 plays a significant role in many essential biological processes, which include regulation of cell cycle, DNA repair, apoptosis, and senescence [501-505]. It has been found that p53 is among the commonly mutated proteins in human tumors because of its highly potent tumor suppressor role. Nearly 50% of human cancers have modifications in the p53 gene, causing inactivation or loss of p53 protein. Moreover, p53 function is effectively inhibited even in cancer cells retaining wild-type p53 [502, 506]. This type of p53 function inhibition is carried out by the MDM2 protein.

MDM2 is an oncoprotein, discovered by its over expression in a spontaneously transformed mouse cancer cell line [502, 506-509]. MDM2 is known to exhibit both p53-independent and p53-dependent functions. Considering the p53 dependent manner, MDM2 directly binds to p53, forms a complex with it, and then inhibits transactivation of p53. Moreover, it has also been found that there are two other sites of interaction between p53 and MDM2: one is between the AD of MDM2 and the DBD of p53, and the other is between the NTD of MDM2 and the CTD of p53. An extensive amount of data has confirmed that MDM2 plays the central role in the p53 pathway.

In normal cells, the activity and protein levels of p53 are controlled by MDM2 via an auto-regulatory loop. p53 activation transcribes mRNAs of MDM2, resulting in an increase in the number of MDM2 proteins, which results in inhibition of p53 activity [510]. MDM2 is a ubiquitously expressed protein and known for its role in the development of tissues, whereas p53 provides powerful tumour surveillance mechanism. Deregulation of MDM2/p53 balance leads to the malignant alteration of cells.

Overexpression of MDM2 result in cells with a growth advantage, supports tumorigenesis, and correlates with poorer clinical prognosis and thereby affects the response to cancer therapy [511-517]. The basic finding is that MDM2 inhbits the function of p53 upon binding. This has led to the remarks that MDM2 overexpression and p53 mutations should be mutually exclusive in tumors. Moreover, in a study, gene amplification of MDM2 was found in tumors of 28 different types consisting of more than 3000 tumors, which strongly favored this notion and established a negative correlation between amplification of MDM2 and occurrence of p53 mutations. Hence, MDM2 is considered as therapeutic target in the cancers retaining wild-type p53.

All the characteristics of biomolecules, including protein-protein interactions can be investigated at the molecular to atomic level by means of Molecular Dynamics (MD) simulation [518], which can help us understand the microscopic mechanisms of biological processes. The force field used determines the accuracy of the simulation. In this study, the Assisted Model Building with Energy Refinement (AMBER) ff99SB force field [519] is used in the MD simulation. One of the key issues in MD simulation, as well as drug design, is calculating the BFE between the receptor and the ligand. BFE [520] is the parameter that determines the binding strength between the receptor and the ligand, making its calculation vital for both studying the mechanism of interaction and drug design. There exist certain residues, which act as potential binding sites for drug-like molecules, called hot areas. Drug-like molecules tend to bind to these hot areas in protein-protein interaction surfaces. The determination of such hotspot residues is another key issue in MD simulation and drug design [521, 522]. The efficiency of drug design can be substantially improved by the implementation of precise free energy prediction methods. MM/PBSA [523-530] method is usually used in calculating the absolute BFE due to their high efficiency, along with the normal mode (Nmode) method to estimate the change in entropy. Whereas, MMPBSA is usually used in calculating the relative BFE in the absence of the Nmode method. PRED is a suitable method to obtain hotspot residues in the MM/PBSA method [529-531].

Many *in silico* studies have been performed on p53-MDM2 interaction [532, 533]. Some of the simulation studies have discussed about the initial capture of Phe19, which serves to unlock the binding cleft through crack propagation. The results obtained in these studies could explain why the F19A p53 mutant does not bind to MDM2 [534]. The detrimental effect of the phosphorylation of p53 Thr18 [535], p53 Ser20 [536], and

MDM2 Ser17 [537], in the p53-MDM2 complex have also been extensively studied using MD and Brownian dynamics (BD) [538]. The studies have also confirmed that p53 predominantly interacts with the NTD of MDM2 via its TAD1. The crystal structure of MDM2 complexed with TAD1 of p53 shows the interaction mediated by three critical residues (Phe19, Trp23, and Leu26) of p53 [539]. The p53–MDM2 interaction was chosen as the model system to validate the computational alanine scanning technique [540-542] and the computed BFE change upon alanine mutation of the p53 peptide residues agreed qualitatively with the experimental data. Phe19, Trp23, Leu26, and Leu22 of p53 were found to play critical role in forming the complex with MDM2. Some of the comprehensive computational studies like enhanced sampling techniques, US and variational free energy profile methods have emphasized on the effect of ligand binding on the structure and dynamics of the N-terminal lid region of MDM2 [543]. The p53–MDM2 interaction was one of the first to be targeted by stapled peptides, the most successful of which has reached clinical trials [544]. Computational methods have played a significant role in understanding the mechanism of stapled peptide binding to MDM2 and also the design of new stapled peptide inhibitors of MDM2 [545]. In 2016, Markov State Models (MSMs) of apo-MDM2 were constructed from large collections of unbiased simulation trajectories to find strong evidence for diffuse, yet two-state folding and binding of the N-terminal region to the p53 receptor site [546]. In the recent past, using replica exchange molecular dynamics (REMD) and Markov State Model (MSM), the conformational distribution and kinetics of p53 N-terminal TAD2, its dual-site phosphorylated form (pSer46, pThr55) were studied [547]. And also a simple four-state kinetic model was parameterized using microscopic rate information from the MSM in order to predict the binding mechanisms, pathways, and rates of p53-MDM2 complex [548]. The dissociation pathways of the complex of MDM2 protein and the TAD of p53 protein (TAD1) were efficiently generated without applying force bias with parallel cascade selection molecular dynamics (PaCS-MD) and showed that PaCS-MD when combined with the Markov State Model (MSM) resulted in a BFE comparable to experimental values [549]. The energy landscape of the total mutagenesis of MDM2 was also determined to identify highly mutable and constrained sites within the protein. For the computational analysis, MUMBO was used to rotamerize the p53-MDM2 crystal structure (PDB ID: 1YCR) to obtain the point mutations [550]. The weighted ensemble path sampling strategy was used to co-ordinate molecular dynamics simulations, generating atomistic views of protein–peptide binding pathways involving the MDM2

oncoprotein and an intrinsically disordered p53 peptide [551]. A quite a number of computational studies [530, 540, 550, 552, 553] have been carried out earlier to determine the BFE for the p53-MDM2 complex and the values have been found to be near to the experimental BFE values (-6.4 to -9.0 kcal mol^{-1}) [554, 555]. The p53-MDM2 interaction has also been studied by considering the complex as a CABS coarse-grained protein model that utilizes a Monte Carlo (MC) sampling scheme and a knowledge-based statistical force field [556]. The conformational landscapes of MDM2-binding p53 peptides were characterized using replica exchange molecular dynamics (REMD) simulations [557].

In the present study, the probable binding and unbinding pathways of the TAD1 of p53 and MDM2 during the formation and dissociation of the p53-MDM2 complex have been determined in terms of the PMF using two different force fields. We have also investigated the conformational dynamics and stability of the TAD1 of the p53 molecule as a function of its center of mass (CoM) distance from MDM2. We also carried out BFE and PRED analyses to infer the binding characteristics and identify hotspot residues across the interface of the p53-MDM2 complex.

For the BFE and PRED analyses, we have used MM/PBSA and MM/GBSA methods [523-531] using *MMPBSA.py* script of the AMBER software package. This method is considered to be one of the popular approaches owing to their modular nature to calculate the free energy of binding of small molecules to a bio-molecule. This method provides better results as it allows the user to adopt flexible and appropriate values for the complex system under study in relation to the dielectric constant, parameters for the non-polar energy, thermodynamic approximations, the radii used for the PB or GB calculations, whether to include the entropy term and whether to perform MD simulations or minimizations. And also it provides instinctive mechanism for predicting the ligand and receptor covers of a complex based on the topology files provided and analyses topology files for parameter constancy. This *MMPBSA.py* script was also reported as an efficient program for end state free energy calculations [558]. For the better results, in this MMPBSA.py script, a more detailed estimates of non-polar energies have been implemented by considering a new non-polar solvation term, that comprises of a (repulsive) cavitation term and a (attractive) dispersion term [559-564].

4.3. Materials & Methods:

4.3.1. Preparation of the p53(TAD1)-MDM2(NTD) system:

The initial 3-D structure of the MDM2 bound to the TAD of p53 complex was obtained from RCSB PDB, bearing the PDB ID: 1YCR. The p53 and MDM2 structures were separated from the p53-MDM2 complex, using UCSF Chimera v.1.13.1. Using the AMBER ff99SB force field, the initial coordinate and the topology file for the separated p53 and MDM2 structures were generated using the Leap module of the AMBER 14 software package. Then, p53 and MDM2 were loaded together, followed by the preparation of the coordinate and topology files of the loaded p53-MDM2 complex in both implicit and explicit environments using the Leap module. The loaded system was solvated with TIP3P [565] water model with a solvent buffer of 10 Å in all directions. The charge of the complex was then neutralized by adding appropriate numbers of counter ions.

Then the p53-MDM2 complex was minimized using AMBER 14 software package in two stages, wherein, it was first subjected to 500 steps of steepest descents minimization (by keeping restraints over the solute) followed by 500 steps of conjugate gradient minimization (devoid of restraints on the solute).

4.3.2. MD simulation of p53(TAD1)-MDM2(NTD) complex:

The MD study was carried out using a standard procedure, which consisted of heating dynamics followed by density, equilibration, and production dynamics. We used a minimized system as our starting structure for subsequent MD steps. The p53-MDM2 system was gradually heated from 0-300 K in constant volume (NVT) conditions, after which the density procedure was carried out. The equilibration of our system was carried out in NPT conditions (300 K and 1 atm pressure) for 1 ns. To ensure successful equilibration of the system, the density, temperature, pressure, and energy graphs were plotted and analyzed. Next, we performed 5 ns MD production run for the equilibrated structure of the p53-MDM2 system using the Particle Mesh Ewald (PME) algorithm [566, 567] with a time step of 2 fs. A cut-off of 8 Å was set to treat the nonbonding interactions (short-range electrostatic as well as van der Waals interactions) during the simulation,

while the long-range electrostatic interactions were treated with the PME method. All the bonds present in the system were constrained using the SHAKE algorithm [568]. The pressure and temperature (0.5 ps of heat bath and 0.2 ps of pressure relaxation) were kept constant by the Berendsen weak coupling algorithm [569] throughout the simulation process.

After completion of the 5 ns of production dynamics of the p53-MDM2 complex, the lowest energy conformer of the complex was extracted out using the RMSD clustering algorithm from the highly populated clusters, followed by the measurement of the CoM distance between p53 and MDM2 in the complex structure. The extracted structure was then used as the initial structure for PMF [570] analysis.

4.3.3. PMF Calculation:

The PMF of the p53-MDM2 complex was calculated using the equilibrium US simulations combined with the WHAM [571, 572]. The free energy profile for the p53-MDM2 complex was traced out conducting US simulations. The analysis of phase space in US relies on MD simulations over a set of regions (windows) that are spread along a predefined direction of reaction. Biasing potentials are generally added to the Hamiltonian to limit the molecular system around the selected regions of phase space. This is carried out in a number of windows along the path of the reaction. In each window, simulations of fixed time interval are carried out and the biased probability distribution (histogram) is obtained.

The WHAM is therefore used to determine the optimal free energy constants for the combined simulations. To study the extent of association of p53 and MDM2 in the p53-MDM2 complex, we calculated the PMF by changing the CoM distance between p53 and MDM2 in the complex. Initial configurations for the different windows of US MD simulation for the p53-MDM2 complex was generated by performing CoM distance constrained MD simulations. The distance between CoMs of the p53 and MDM2 was changed with time from 7 to 26 Å spanning different configurations. At each window of US, the system was carried out for a 10 ns time period of MD simulation with harmonic potentials to maintain the CoM distance between the two molecules near the desired values.

After every MD run, the trajectories generated were visualized by the means of VMD package [573]. At large separation of p53 and MDM2 in the complex, the PMF data was normalized by means of centering and standard deviation method. RMSD, DSSP, probability score of secondary structure, and intramolecular hydrogen bond analyses were performed for p53 only for all the increasing and decreasing coordinates.

4.3.4. MD simulation of the lowest energy structure of the p53-MDM2 complex:

From the ensemble of the p53-MDM2 complex structures at the reaction co-ordinate corresponding to the minimum PMF value, a structure of lowest potential energy was selected and then subjected to MD simulation in order to study its salient structural features. Minimization, heating, density, equilibration, and production dynamics were carried out using the same standard procedure used above, but with a change in the duration of the production run. The production dynamics were run for 100 ns. The MD trajectories for the complex were analysed using the PTRAJ (short for Process TRAJectory) and CPPTRAJ (a rewrite of PTRAJ in C++) modules [574] of AMBER 14 Tools. To evaluate the convergence of our system, we studied the RMSDs for p53, MDM2, and the p53-MDM2 complex, wherein the starting structure of MD was used as the reference. We also calculated the RMSFs to analyze the flexibility of both protein complexes. In addition, Rg, SASA, and intra/inter-molecular hydrogen bond analyses were also performed for p53, MDM2, and p53-MDM2 complex in order to understand how the stability of the p53-MDM2 complex is affected during the course of MD simulation.

4.3.5. Determination of the interface residues:

For the determination of the PPI of p53-MDM2, we have pulled out the lowest potential energy structure of the p53-MDM2 complex from ensemble of the p53-MDM2 complex structures at the reaction co-ordinate corresponding to the minimum PMF value. The resultant lowest energy structure was then uploaded in the PDBsum server to visualize the intermolecular interface residues of p53-MDM2. The residues of a protein whose contact CoM distances from its interacting protein partner are less than 6 Å are called the

interface residues [575].

4.3.6. BFE analyses for the p53(TAD1)-MDM2(NTD) complex:

The relative BFE and the PRED of the interface residues of the p53-MDM2 complex in this present study were acquired using MMPBSA.py script of the AMBER 14 suite. This script is based on the MM/PBSA and MM/GBSA algorithms. The MM-PBSA/GBSA methods were utilized to determine the BFE (ΔG_{bind}/$\Delta G_{binding}$) and to understand the contributions from electrostatic and van der Waals terms in the formation of complexes. The PRED analysis provides the energy contribution from each residue of a protein by studying its molecular interactions over all residues in the system/complex. All the trajectories were taken into consideration for the MM-PBSA/GBSA calculations. The free energy analyses are considered important in establishing the binding affinity in the protein-protein, ligand-protein, DNA-protein, and DNA-ligand interaction studies. Hence, to gather the differences in the binding affinities of our system (p53-MDM2 complex), the MM-PBSA/GBSA analysis was done for our system by considering the following components (i) p53 (ligand), (ii) MDM2 (receptor) and (iii) p53-MDM2 (complex).

The BFE of $p53_{ligand}$ - $MDM2_{receptor}$ = $p53\text{-}MDM2_{complex}$ was calculated using Equation 4.1, derived from the second law of thermodynamics, where studies were conducted in both gas (vacuum) and aqueous environments.

$$\Delta G_{binding} = \Delta G_{complex} - [\Delta G_{receptor} + \Delta G_{ligand}] \qquad (4.1)$$

where, $\Delta G_{binding}$ is the final estimated BFE calculated by using the MM-PBSA algorithm. According to the second law of thermodynamics, $\Delta G_{binding}$ can be decomposed into enthalpy (ΔH) and entropy ($-T\Delta S$) (Equation 4.2). Here the enthalpies were calculated by both MM-GBSA and MM-PBSA methods with a modest computational effort [576] and the entropy was estimated with normal mode (nmode) analysis.

Thermodynamically,

$$\Delta G_{binding} = H - T\Delta S \qquad (4.2)$$

$$\Delta G_{binding} = \Delta G_{gas} + \Delta G_{solv} - T\Delta S \quad (4.3)$$

$$\Delta G_{gas} = \Delta E_{EL} + \Delta E_{VDWAALS} \quad (4.4)$$

$$\Delta G_{solv} = \Delta E_{GB/PB} + \Delta E_{SURF} \quad (4.5)$$

$$\Delta E_{SURF} = \Delta E_{NPOLAR} + \Delta E_{DISPER} \quad (4.6)$$

The enthalpy part is calculated by summation of total gas-phase energy (ΔG_{gas}) and solvation- free energy (ΔG_{solv}) as shown in Equation 4.3. ΔG_{gas} is composed of electrostatic interaction (ΔE_{EL}) and van der Waals interaction ($\Delta E_{VDWAALS}$) (Equation 4.4). The solvation-free energy is divided into polar ($\Delta E_{GB/PB}$) and non-polar (ΔE_{SURF}) contributions (Equation 4.5). ΔE_{GB} is calculated by Generalized Born model, ΔE_{PB} is calculated by the Poisson-Boltzmann model, and ΔE_{SURF}, in case of PB model, is the summation of non-polar contribution calculated by PB (ΔE_{NPOLAR}) and dispersion energy (ΔE_{DISPER}) using Solvent Accessibility Surface Area (SASA) (Equation 4.6).

4.4. Results & Discussions:

4.4.1. PMF profile of p53(TAD1)-MDM2(NTD) complex:

We have conducted a PMF study by combining MD simulations with the US method [577] to examine the degree of association of p53 with MDM2 in forming the complex. The PMF profile for p53-MDM2 complex in the water at room temperature as a function of reaction coordinate has been shown in **Figure 4.1**. Here the reaction co-ordinate is described as the distance between the centers of mass of p53 and MDM2. From **Figure 4.1**, we see the presence of a minimum PMF value of p53-MDM2 complex at a distance of separation of 12 Å with the dissociation energy of 30 kcal mol^{-1}. We observed p53 and MDM2 to show no more interactions when the distance of separation between them crosses 22 Å. But when the inter-chain distance between p53 and MDM2 was decreased from the optimum distance of 12 Å, we noticed the PMF to increase because of repulsive forces between p53 and MDM2. To ensure the PMF profile of p53-MDM2 complex, we have carried out the MD simulations of this complex using another force field (ff99SB-ILDN) and obtained almost the similar PMF profile (as depicted in the **Figure 4.2**).

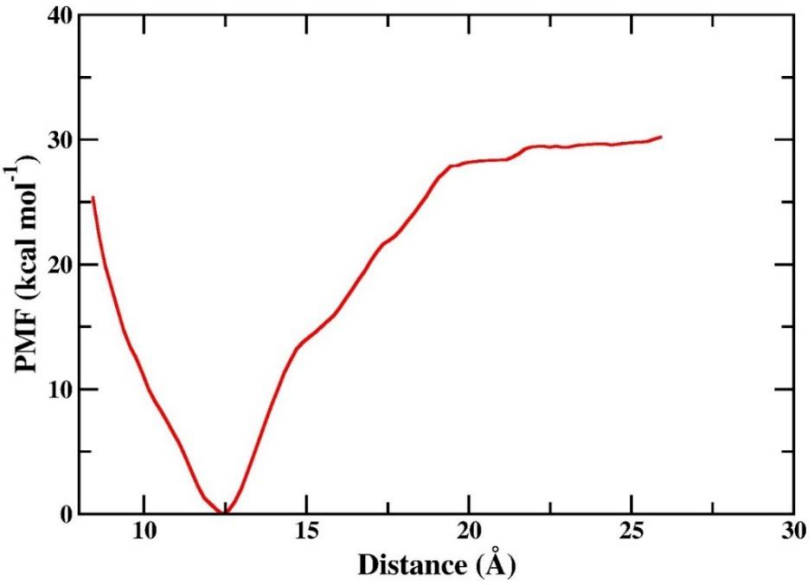

Figure 4.1. *Potential of Mean Force as a function of the reaction coordinate for the association and dissociation of the p53-MDM2 complex using force field ff99SB.*

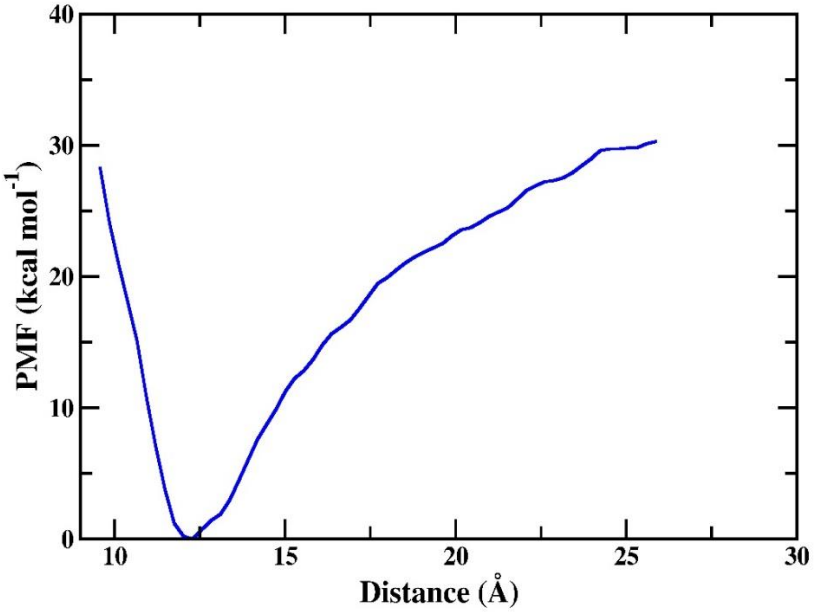

Figure 4.2. *Potential of Mean Force as a function of the reaction coordinate for the association and dissociation of the p53-MDM2 complex using force field ff99SB-ILDN.*

4.4.2. Analysis of conformational dynamics of p53 as a function of its CoM distance from MDM2:

During the US simulation of the p53-MDM2 complex, we found p53 to undergo rapid change in its conformational dynamics. The snapshots of the p53-MDM2 complex obtained at different windows of the distance of separation as defined by the reaction coordinate were shown in **Figure 4.3**. The snapshots have been constructed using UCSF

Chimera v.1.13.176 [578]. Distinct colors have been used to depict the secondary structure portions of the p53-MDM2 complex. We observed the helical portion present in p53 to decrease with its distance of separation from MDM2.

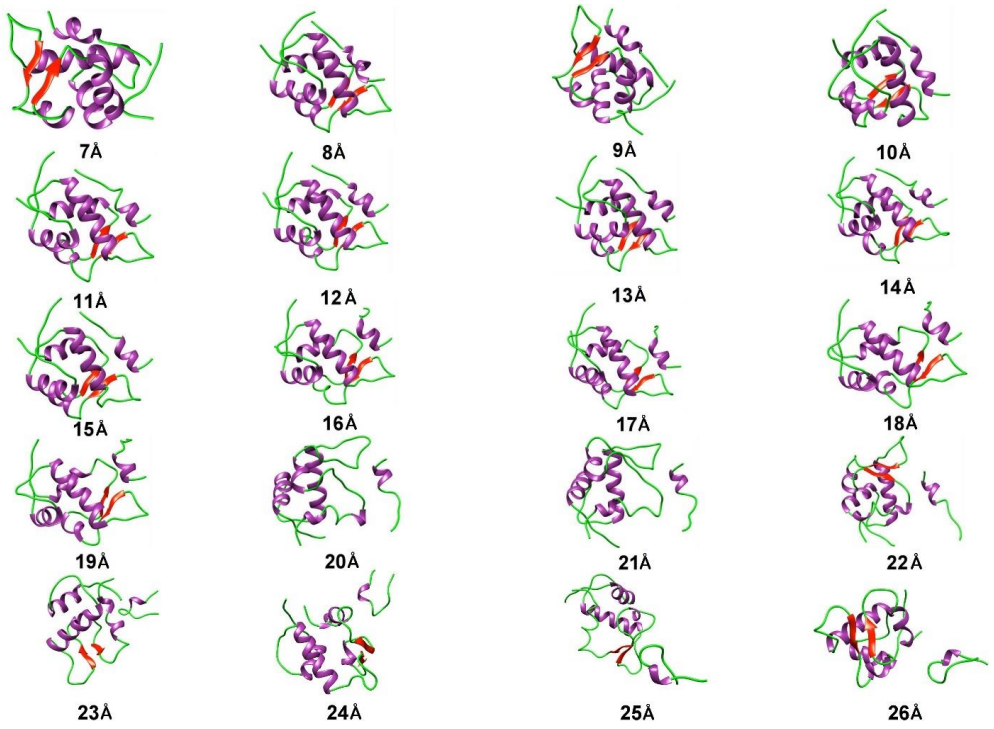

Figure 4.3. *Snapshots of p53-MDM2 complex structures at discrete distance of separation (in Å) from MDM2 (purple color = helices, green color = coils, red color = strands).*

4.4.3. RMSD analysis for p53 as a function of its CoM distance from MDM2:

We have carried out the RMSD analysis to know the structural stability of p53 in the p53-MDM2 complex during the course of US simulation. **Figure 4.4a** represents the RMSD analysis for the p53 molecule in the complex when the inter-chain distance between p53 and MDM2 is decreased from the optimum distance of 12 Å to 7 Å. **Figure 4.4b** represents the RMSD analysis for the p53 molecule in the complex when the inter-chain distance between p53 and MDM2 is increased from the optimum distance of 12 Å to 26 Å. From **Figure 4.4a**, it can be seen that p53 undergo changes in its conformation more rapidly when it is pushed more towards MDM2 from its optimum distance. This is because of an increase in strong van der Waals forces with a decrease in distance between p53 and MDM2. From **Figure 4.4b**, it can be observed that p53 holds different foldings at different intervals of distance from MDM2 when it is pulled away from its optimum distance. p53 was initially observed to take a fold that is maintained until the distance of

separation from MDM2 reaches 17 Å. At 17 Å the p53 takes a new fold and that is maintained till the distance of separation reaches 22 Å. But when the distance of separation between p53 and MDM2 crosses 22 Å, p53 shows no more interaction with MDM2 and therefore it shows rapid changes in its conformation. As a whole we have monitored the different folding patterns of p53 during the course of its separation from MDM2. These folding pattern inferences are very much important to design the methods of inhibition for p53-MDM2 complex.

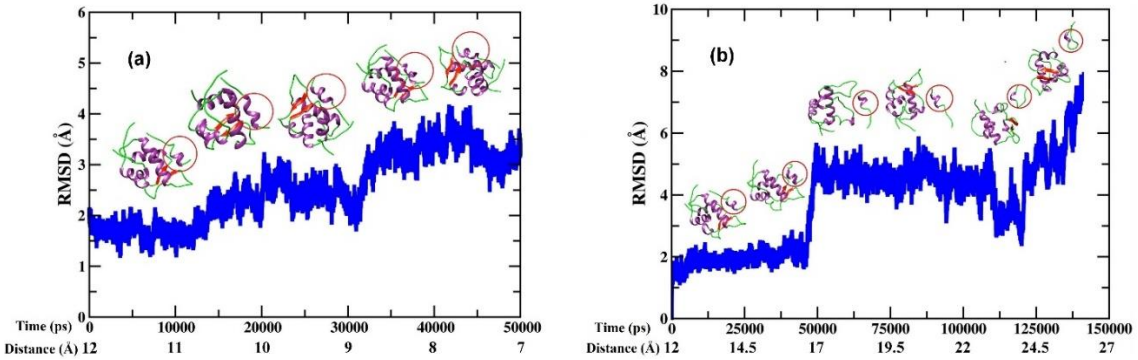

Figure 4.4. *RMSD analysis for p53 molecule when the distance of separation between p53 and MDM2 (a) decreased from 12 Å to 7 Å; (b) increased from 12 Å to 26 Å.*

4.4.4. DSSP analysis of p53 as a function of its CoM distance from MDM2:

We then performed the DSSP [579] analysis using the Kabsch and Sander algorithm [580] to investigate the changes in secondary structural elements in the p53 molecule. **Figure 4.5a** depicts the secondary structural changes in p53 molecule when the inter-chain distance between p53 and MDM2 is decreased from the optimum distance of 12 Å to 7 Å. **Figure 4.5b** represents the secondary structural changes in p53 molecule when the inter-chain distance between p53 and MDM2 is increased from the optimum distance of 12 Å to 26 Å. From **Figure 4.5a**, it can be seen that there is an increase in the 3_{10}-helix content of p53 with a decrease in the distance of separation between p53 and MDM2. The secondary structural transition from $\alpha/3_{-10}$ helix to turns have been observed in p53 with an increase in distance of separation between p53 and MDM2 (**Figure 4.5b**). But when the distance of separation between p53 and MDM2 crosses 22 Å, p53 shows no more interaction with MDM2 and therefore it shows marked changes in its conformation and found to contain more turns instead of helical content.

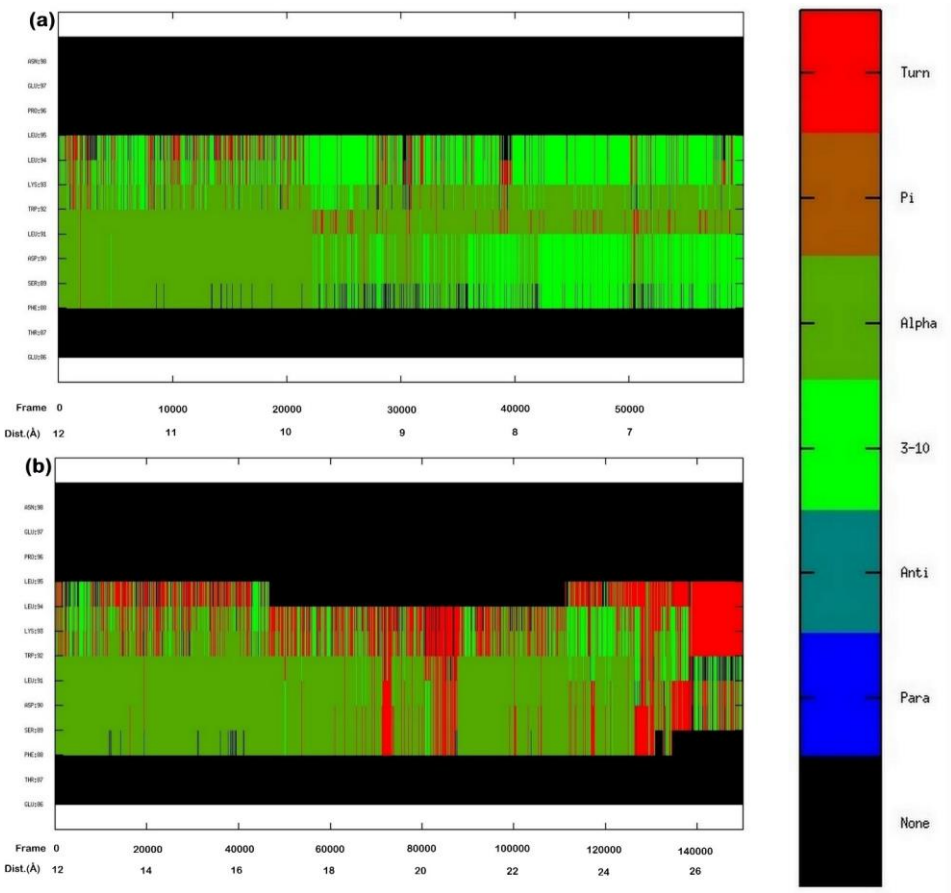

Figure 4.5. *The evolution of secondary structure evaluated using DSSP is shown for p53 molecule when the distance of separation between p53 and MDM2 (a) decreased from 12 Å to 7 Å; (b) increased from 12 Å to 26 Å. Y-axis depicts p53 residues and X-axis depicts time frames as well distance of separation of p53 from MDM2. The secondary structure components of p53 are color-coded as shown in the panel.*

4.4.5. Analysis of probable secondary structure per residue of p53 as a function of its CoM distance from MDM2:

Then we carried out the analysis of the probable secondary structure that can be retained by each residue of p53. **Figure 4.6a** represents the probability score versus residue index for the p53 molecule when the inter-chain distance between p53 and MDM2 is decreased from the optimum distance of 12 Å to 7 Å. **Figure 4.6b** represents the probability score versus residue index for the p53 molecule when the inter-chain distance between p53 and MDM2 is increased from the optimum distance of 12 Å to 26 Å. From **Figure 4.6a**, we observe that the p53 molecule contains the secondary structure α-helix and 3_{10}-helix predominantly in the region 87 to 95. We also noticed turns with fewer probability scores in the region 92 to 95. From **Figure 4.6b**, we see p53 molecule to contain α-helical secondary structure with a higher probability score in the region 87 to 95. But we also

observed the secondary structure turn to evolve with a higher probability score than 3_{10}-helix in the region 87 to 95. This is because when the distance of separation between p53 and MDM2 crosses 22 Å, p53 shows no more interaction with MDM2 and therefore it shows marked changes in the secondary structure resulting in the increase in turns content and decrease in the α-helical as well as 3_{-10} helix content.

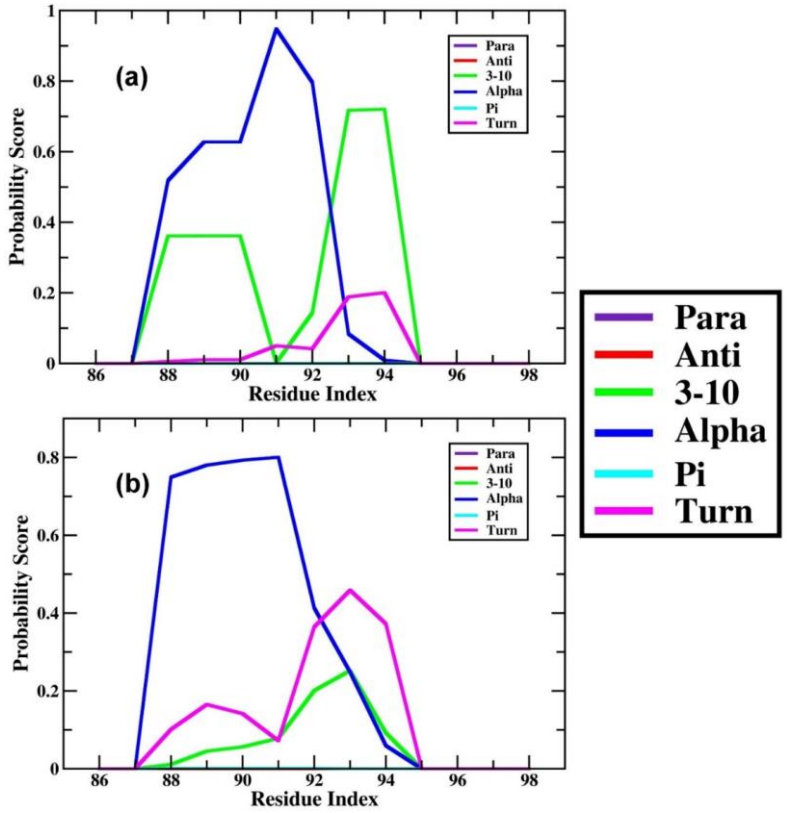

Figure 4.6. *Probability score for secondary structure analysis for p53 when the distance of separation between p53 and MDM2 (a) decreased from 12 Å to 7 Å; (b) increased from 12 Å to 26 Å.*

4.4.6. Intramolecular hydrogen bond analyses for p53 as a function of CoM distance:

Using the trajectory files generated from each window during the PMF analysis, we have performed the intramolecular hydrogen bond analysis for p53. In **Figures 4.7a** and **4.7b,** the intramolecular hydrogen bond analysis for p53 molecule was shown as a function of the inter-chain distance (by decreasing and increasing from its optimum distance) between p53 and MDM2. From **Figure 4.7a** and **4.7b**, we see that the number of intramolecular hydrogen bonds present in p53 molecule to increase evidently when the interchain

distance between p53 and MDM2 increases or decreases from the optimum distance of 12 Å. This is because p53 molecule experience varied binding affinity from MDM2 as the distance between them changes.

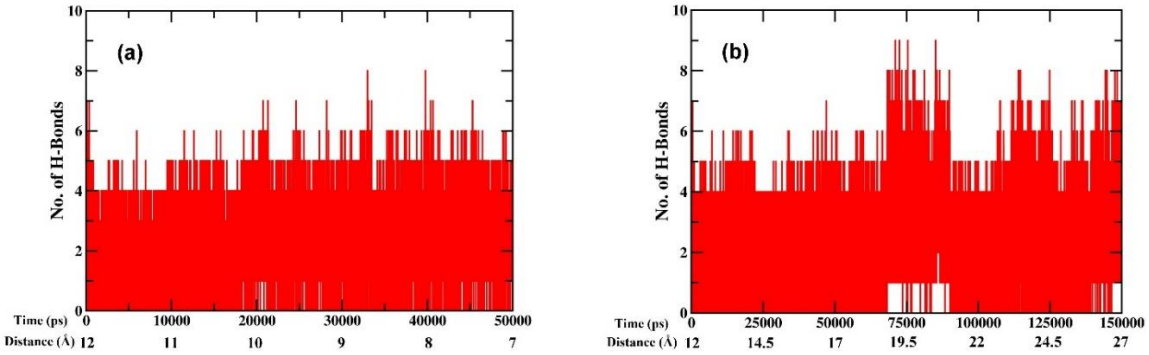

Figure 4.7. *Intra-molecular hydrogen bond analysis for p53 when the distance of separation between p53 and MDM2 (a) decreased from 12 Å to 7 Å; (b) increased from 12 Å to 26 Å.*

4.4.7. Density, temperature, pressure, potential energy, kinetic energy and total energy of the p53-MDM2 complex:

The minimum PMF structure of the p53-MDM2 complex was isolated from the PMF analysis and then subjected to molecular dynamics simulation for 100 ns to study the salient structural features of the p53-MDM2 complex: RMSD, RMSF, Rg, Solvent Accessible Surface Area (SASA), Hydrogen Bond analyses, Protein-Protein Interface Interaction, BFE and PRED analyses. MD simulations yield in-depth knowledge about the dynamic behavior of a particular system that is being studied and help us to understand the changes in their stability and flexibility over the time period. To check the correctness of our NPT simulation algorithm, we have plotted the density, temperature, pressure, potential energy, kinetic energy and total energy of the p53-MDM2 complex as a function of the simulation time period (shown in **Figure 4.8**).

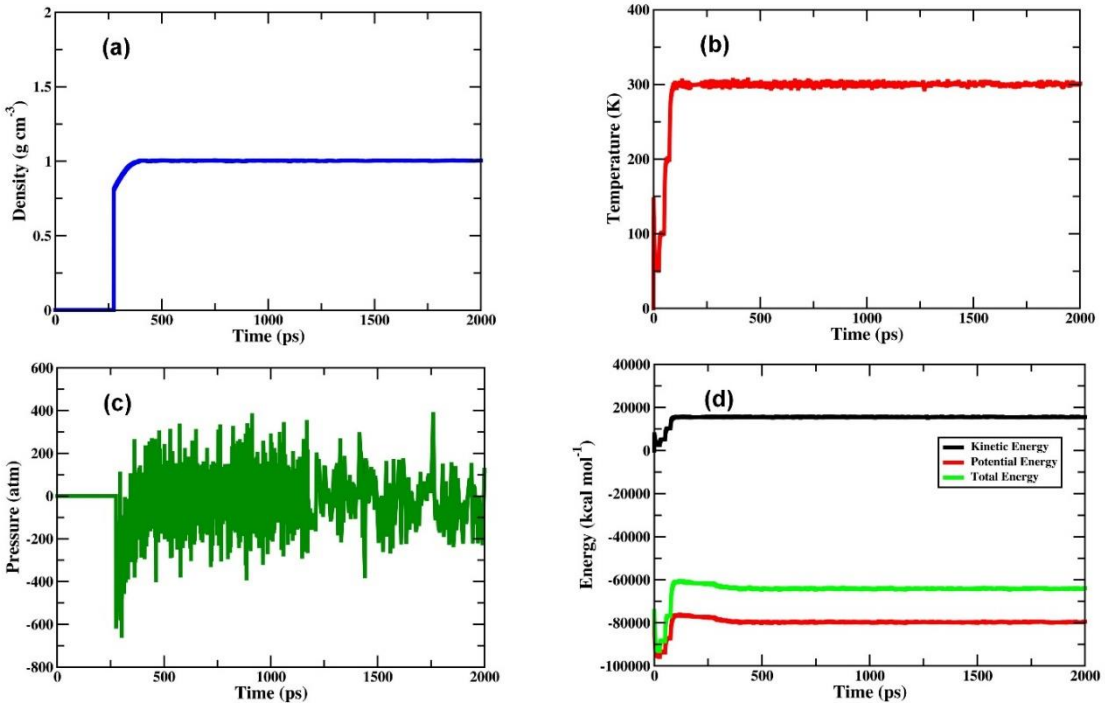

Figure 4.8. *Assessment of stability of MD parameters: (a) Density, (b) Temperature, (c) Pressure, and (d) Energy of p53-MDM2 complex during the equilibration phases of MD simulation.*

4.4.8. RMSD Analysis of the p53(TAD1)-MDM2(NTD) Complex:

In a typical MD simulation, the stability of the system is generally studied by tracking the RMSD of that protein/biological molecule as a function of time. For the p53-MDM2 complex studied here, the RMSD values as a function of time have been shown in **Figure 4.9a**. **Figure 4.9a** shows a comparative RMSD plot for p53, MDM2, and p53-MDM2 complex, where p53, MDM2 and p53-MDM2 complex was observed to have converged at 7500 ps with the average RMSD value of 2 Å, 2.5 Å, and 2.5 Å, respectively.

4.4.9. RMSF Analysis of the p53(TAD1)-MDM2(NTD) Complex:

Residue flexibility of the p53-MDM2 system was evaluated using the RMSF. **Figure 4.9b** shows the RMSF values for C-α atoms of individual p53 and MDM2 in the p53-MDM2 complex with respect to the time evolution of 100 ns trajectories. For the complex, the residue fluctuations were seen for MDM2 between residue numbers 40 and 60, and residue fluctuations were found to be present for N-terminal and C-terminal residues of the p53

chain. The RMSF comparison of the p53 and MDM2 from the p53-MDM2 system revealed that MDM2 shows more number of average residue fluctuations than p53.

4.4.10. Rg Analysis of the p53(TAD1)-MDM2(NTD) Complex:

Rg is generally calculated to assess the total dispersion of atoms in a particular biomolecule from their common center of gravity/axis. The Rg analysis for p53, MDM2, and p53-MDM2 complex are given in **Figure 4.9c**. Here, we observed the Rg values for the p53, MDM2, and p53-MDM2 to oscillate within the mean value of 8 Å, 13 Å, and 13 Å, respectively. The curves for p53, MDM2, and p53-MDM2 are seen to be settled throughout the entire course of production dynamics. The profile trend we see in the Rg values for each structure are the reflections endured by each structure because of their intermolecular interactions during the course of the simulation.

4.4.11. SASA Analysis of the p53(TAD1)-MDM2(NTD) Complex:

Overall variations in the total SASA of p53, MDM2, and p53-MDM2 are shown in **Figure 4.9d**. The SASA values reflects all the unsuitable (hydrophobic) contacts between the water molecules and biomolecules. To determine the surface area accessible by the water solvent for the p53-MDM2 system, a probe with a radius of 1.4 Å was used. The SASAs of the p53 and MDM2 remained constant at 1000 $Å^2$ and 5000 $Å^2$, respectively. However, SASA for the p53-MDM2 complex fluctuated around 6000 $Å^2$. Thus, more the number of residues; more is the number of hydrophobic contacts possible, resulting in a higher SASA value.

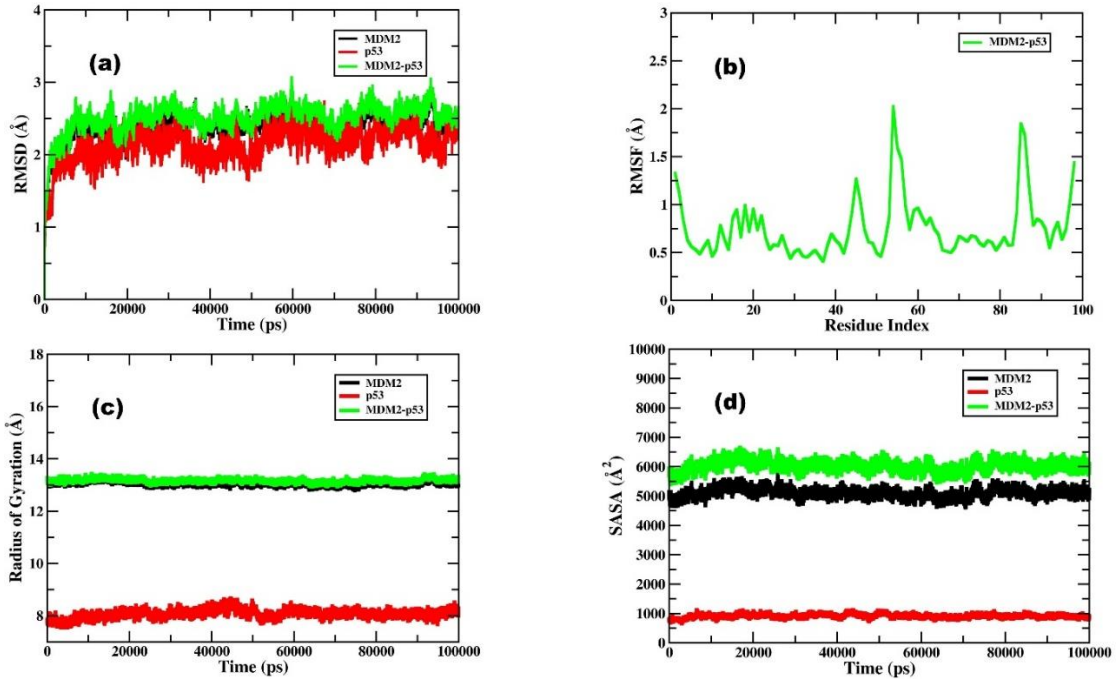

Figure 4.9. *The structural characteristics (a) Root Mean Square Deviation (RMSD), (b) Root Mean Square Fluctuation (RMSF), (c) Radius of Gyration (Rg), and (d) Solvent Accessible Surface Area (SASA) of p53, MDM2, and the complex during 100 ns Molecular Dynamics simulation.*

4.4.12. Hydrogen Bond Analysis of the p53(TAD1)-MDM2(NTD) Complex:

Additionally, we also calculated the number of intramolecular hydrogen bonds present in p53 and in MDM2, as well as the number of intermolecular hydrogen bonds present in the p53-MDM2 complex to analyse the stability of the protein complex. The hydrogen bonds obtained were shown in **Figure 4.10** and found to contain the values within the ideal range as proposed for globular proteins [581]. An average of thirty-five hydrogen bonds was found to be present in MDM2 (**Figure 4.10a**), an average of three hydrogen bonds was found to be present in p53 (**Figure 4.10b**) and an average of five inter-molecular hydrogen bonds was found to be seen in the p53-MDM2 complex (**Figure 4.10c**).

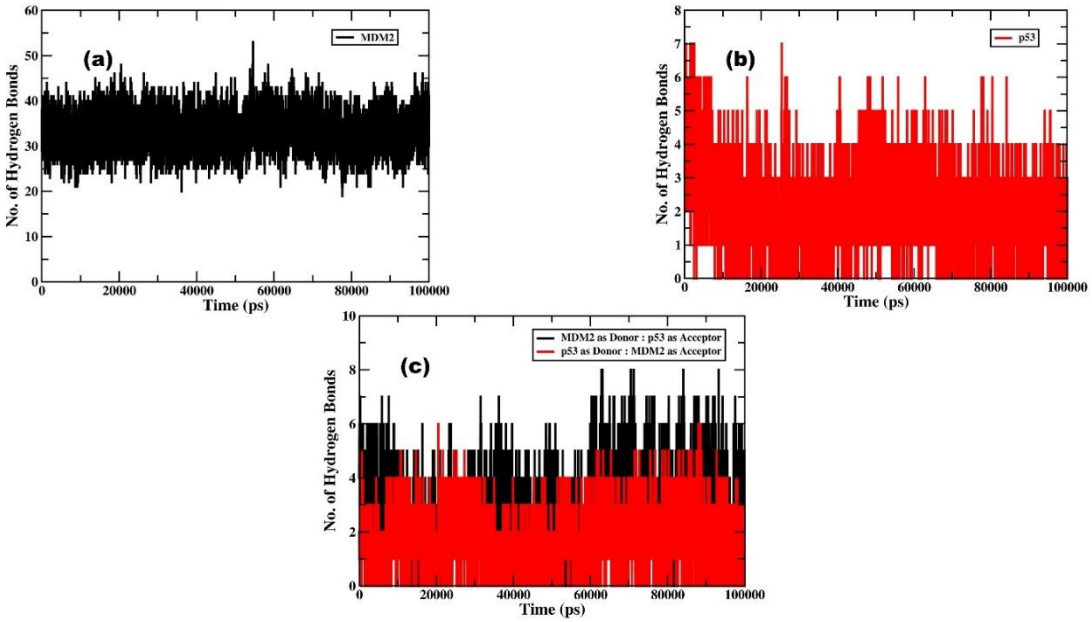

Figure 4.10. *Intra-molecular hydrogen bond analysis of (a) MDM2, and (b) p53; and (c) intermolecular hydrogen bond analysis for the p53-MDM2 complex structure.*

4.4.13. Determination of the interface interactions of the p53(TAD1)-MDM2(NTD) Complex:

An interface area is generally defined as a region where two sets of proteins come into contact with each other. Surface residues with large surface regions accessible to the solvent available usually characterize them. The interface statistics for the p53-MDM2 complex were obtained upon the submission of the lowest energy structure of the p53-MDM2 complex extracted from the PMF analysis to the PDBsum server [582]. The interface statistics have been shown in **Table 4.1**. The summarized intermolecular interactions between p53 and MDM2 of the p53-MDM2 complex at the residue levels are shown in **Figure 4.11**. The comprehensive contributions of each interface residue stabilizing the p53-MDM2 complex are accordingly given in **Table 4.2**. The total number of interface residues in the p53-MDM2 complex was found to be twenty-seven. The interface area for the MDM2 chain and the p53 chain involved in the interaction was observed to be 660 $Å^2$ and 809 $Å^2$ respectively. The docked complex was stabilized by molecular interactions like salt bridges, hydrogen bonding, and non-bonded contacts. According to **Figure 4.11**, eighty-four non-bonded interactions are present along with one salt bridge and three hydrogen bonds between MDM2 and p53. Sixteen residues from

MDM2 and eleven residues from p53 are involved in the interaction between MDM2 and p53. The three hydrogen bonds and the single salt bridge present aid the stability of the p53-MDM2 complex. It can be seen that Gln72, Leu54, and Thr26 of MDM2 form hydrogen bonds with Glu17, Trp23, and Asn29 of p53, respectively. Another key observation is that Lys94 of MDM2 forms a salt bridge with Glu17 of p53 in the complex which is the only key difference between the interface statistics of the lowest energy p53-MDM2 structure and the experimentally determined p53-MDM2 complex structure present in the RCSB PDB [583], bearing the PDB ID: 1YCR.

Table 4.1. Interface statistics for the minimum PMF structure of the p53-MDM2 complex.

Chain	No. of Interface Residues	Interface Area (Å^2)	No. of Salt Bridges	No. of Disulphide Bonds	No. of Hydrogen Bonds	No. of Non-Bonded Contacts
MDM2	16	660	1	-	3	84
p53	11	809				

Table 4.2. List of atom-atom interactions across p53-MDM2 interface.

Salt bridges

	<----- MDM2 ----->					<----- p53 ----->					
	Atom no.	Atom name	Res name	Res no.	Chain		Atom no.	Atom name	Res name	Res no.	Chain	Distance
1.	570	NZ	LYS	94	A	<-->	714	OE1	GLU	17	B	3.40

Hydrogen bonds

	<----- MDM2 ----->					<----- p53 ----->					
	Atom no.	Atom name	Res name	Res no.	Chain		Atom no.	Atom name	Res name	Res no.	Chain	Distance
1.	15	OG1	THR	26	A	<-->	817	OD1	ASN	29	B	3.27
2.	234	O	LEU	54	A	<-->	764	NE1	TRP	23	B	2.83
3.	400	OE1	GLN	72	A	<-->	723	N	PHE	19	B	3.02

Non-bonded contacts

	<----- MDM2 ----->					<----- p53----->					
	Atom no.	Atom name	Res name	Res no.	Chain		Atom no.	Atom name	Res name	Res no.	Chain	Distance
1.	5	CB	GLU	25	A	<-->	817	OD1	ASN	29	B	3.70
2.	8	OE1	GLU	25	A	<-->	817	OD1	ASN	29	B	3.60
3.	8	OE1	GLU	25	A	<-->	818	ND2	ASN	29	B	3.44
4.	15	OG1	THR	26	A	<-->	812	CA	ASN	29	B	3.81
5.	15	OG1	THR	26	A	<-->	817	OD1	ASN	29	B	3.27
6.	15	OG1	THR	26	A	<-->	819	OXT	ASN	29	B	3.76

7.	16	CG2	THR	26	A	<-->	815	CB	ASN	29	B	3.90
8.	16	CG2	THR	26	A	<-->	819	OXT	ASN	29	B	3.42
9.	200	C	MET	50	A	<-->	805	O	GLU	28	B	3.79
10.	202	CB	MET	50	A	<-->	804	C	GLU	28	B	3.74
11.	202	CB	MET	50	A	<-->	805	O	GLU	28	B	3.25
12.	202	CB	MET	50	A	<-->	811	N	ASN	29	B	3.85
13.	202	CB	MET	50	A	<-->	812	CA	ASN	29	B	3.47
14.	203	CG	MET	50	A	<-->	812	CA	ASN	29	B	3.82
15.	203	CG	MET	50	A	<-->	813	C	ASN	29	B	3.73
16.	203	CG	MET	50	A	<-->	819	OXT	ASN	29	B	3.60
17.	205	CE	MET	50	A	<-->	798	O	PRO	27	B	3.29
18.	206	N	LYS	51	A	<-->	805	O	GLU	28	B	3.40
19.	211	CG	LYS	51	A	<-->	805	O	GLU	28	B	3.16
20.	211	CG	LYS	51	A	<-->	806	CB	GLU	28	B	3.68
21.	233	C	LEU	54	A	<-->	764	NE1	TRP	23	B	3.75
22.	234	O	LEU	54	A	<-->	764	NE1	TRP	23	B	2.83
23.	234	O	LEU	54	A	<-->	765	CE2	TRP	23	B	3.57
24.	234	O	LEU	54	A	<-->	767	CZ2	TRP	23	B	3.68
25.	237	CD1	LEU	54	A	<-->	798	O	PRO	27	B	3.24
26.	237	CD1	LEU	54	A	<-->	803	CA	GLU	28	B	3.80
27.	238	CD2	LEU	54	A	<-->	793	CD1	LEU	26	B	3.88
28.	270	N	GLY	58	A	<-->	764	NE1	TRP	23	B	3.79
29.	271	CA	GLY	58	A	<-->	764	NE1	TRP	23	B	3.49
30.	271	CA	GLY	58	A	<-->	765	CE2	TRP	23	B	3.74
31.	273	O	GLY	58	A	<-->	732	CE2	PHE	19	B	3.72
32.	299	CB	ILE	61	A	<-->	733	CZ	PHE	19	B	3.71
33.	301	CG2	ILE	61	A	<-->	731	CE1	PHE	19	B	3.79
34.	301	CG2	ILE	61	A	<-->	733	CZ	PHE	19	B	3.47
35.	302	CD1	ILE	61	A	<-->	733	CZ	PHE	19	B	3.75
36.	302	CD1	ILE	61	A	<-->	768	CZ3	TRP	23	B	3.86
37.	308	CG	MET	62	A	<-->	730	CD2	PHE	19	B	3.30
38.	308	CG	MET	62	A	<-->	732	CE2	PHE	19	B	3.65
39.	309	SD	MET	62	A	<-->	739	OG	SER	20	B	3.25
40.	310	CE	MET	62	A	<-->	730	CD2	PHE	19	B	3.76
41.	310	CE	MET	62	A	<-->	732	CE2	PHE	19	B	3.65
42.	310	CE	MET	62	A	<-->	739	OG	SER	20	B	3.09
43.	393	N	GLN	72	A	<-->	715	OE2	GLU	17	B	3.52
44.	396	O	GLN	72	A	<-->	729	CD1	PHE	19	B	3.63
45.	397	CB	GLN	72	A	<-->	710	O	GLU	17	B	3.49
46.	397	CB	GLN	72	A	<-->	718	C	THR	18	B	3.83
47.	397	CB	GLN	72	A	<-->	723	N	PHE	19	B	3.40
48.	398	CG	GLN	72	A	<-->	710	O	GLU	17	B	3.51
49.	399	CD	GLN	72	A	<-->	723	N	PHE	19	B	3.90
50.	400	OE1	GLN	72	A	<-->	717	CA	THR	18	B	3.60
51.	400	OE1	GLN	72	A	<-->	718	C	THR	18	B	3.79
52.	400	OE1	GLN	72	A	<-->	720	CB	THR	18	B	3.80
53.	400	OE1	GLN	72	A	<-->	723	N	PHE	19	B	3.02
54.	400	OE1	GLN	72	A	<-->	727	CB	PHE	19	B	3.83
55.	402	N	HIS	73	A	<-->	755	CD2	LEU	22	B	3.68
56.	403	CA	HIS	73	A	<-->	755	CD2	LEU	22	B	3.72
57.	406	CB	HIS	73	A	<-->	714	OE1	GLU	17	B	3.73
58.	406	CB	HIS	73	A	<-->	755	CD2	LEU	22	B	3.60
59.	407	CG	HIS	73	A	<-->	714	OE1	GLU	17	B	3.85
60.	409	CD2	HIS	73	A	<-->	714	OE1	GLU	17	B	3.44
61.	426	CG2	VAL	75	A	<-->	731	CE1	PHE	19	B	3.85
62.	558	O	VAL	93	A	<-->	794	CD2	LEU	26	B	3.57

63.	560	CG1	VAL	93	A	<-->	731	CE1	PHE	19	B	3.57
64.	560	CG1	VAL	93	A	<-->	766	CE3	TRP	23	B	3.83
65.	561	CG2	VAL	93	A	<-->	752	CB	LEU	22	B	3.33
66.	561	CG2	VAL	93	A	<-->	753	CG	LEU	22	B	3.80
67.	569	CE	LYS	94	A	<-->	714	OE1	GLU	17	B	3.11
68.	570	NZ	LYS	94	A	<-->	714	OE1	GLU	17	B	3.40
69.	586	ND1	HIS	96	A	<-->	782	O	LEU	25	B	3.80
70.	586	ND1	HIS	96	A	<-->	794	CD2	LEU	26	B	3.36
71.	587	CD2	HIS	96	A	<-->	782	O	LEU	25	B	3.69
72.	588	CE1	HIS	96	A	<-->	782	O	LEU	25	B	3.27
73.	588	CE1	HIS	96	A	<-->	794	CD2	LEU	26	B	3.85
74.	589	NE2	HIS	96	A	<-->	782	O	LEU	25	B	3.17
75.	624	CD1	TYR	100	A	<-->	798	O	PRO	27	B	3.90
76.	624	CD1	TYR	100	A	<-->	799	CB	PRO	27	B	3.67
77.	626	CE1	TYR	100	A	<-->	798	O	PRO	27	B	3.63
78.	626	CE1	TYR	100	A	<-->	799	CB	PRO	27	B	3.70
79.	626	CE1	TYR	100	A	<-->	814	O	ASN	29	B	3.36
80.	628	CZ	TYR	100	A	<-->	814	O	ASN	29	B	3.30
81.	629	OH	TYR	100	A	<-->	813	C	ASN	29	B	3.07
82.	629	OH	TYR	100	A	<-->	814	O	ASN	29	B	2.68
83.	629	OH	TYR	100	A	<-->	819	OXT	ASN	29	B	2.81
84.	664	OH	TYR	104	A	<-->	819	OXT	ASN	29	B	3.39
Number of salt bridges: 1												
Number of hydrogen bonds: 3												
Number of non-bonded contacts: 84												

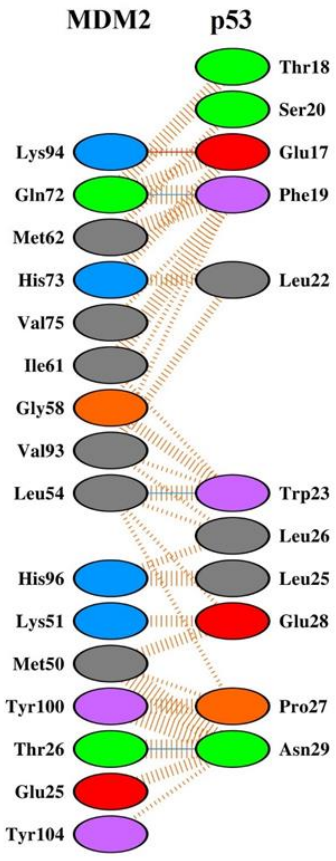

Figure 4.11. *Intermolecular interactions between MDM2 and p53 in the minimum PMF structure of the p53-MDM2 complex.*

4.4.14. BFE and PRED analyses of the p53(TAD1)-MDM2(NTD) Complex:

The BFE calculations of p53 and MDM2 to form the p53-MDM2 complex were done using MM-PBSA/GBSA method. The values here represent only the relative BFE rather than absolute or total binding energy, as MM-PBSA/GBSA utilizes a continuum solvent approach to calculate the BFE of a system. The BFE determined for the p53-MDM2 complex using MM-GBSA and MM-PBSA methods, along with the energy terms, are given in **Table 4.3** and **4.4** respectively.

Table 4.3. *The various components of the BFE (kcal mol^{-1}) evaluated by MM/GBSA method between p53-MDM2 complex.*

	p53-MDM2		MDM2		p53		Delta	
	Average	Std. Dev. (±)	Average	Std. Dev. (±)	Average	Std. Dev. (±)	Average	Std. Dev. (±)
$\Delta E_{VDWAALS}$	-776.69	12.17	-638.49	11.02	-65.47	3.10	-72.72	5.38
ΔE_{EL}	-7415.31	32.88	-5970.25	31.26	-1015.38	16.09	-429.68	16.07
ΔE_{GB}	-1177.75	24.57	-1244.09	23.12	-390.48	12.80	456.82	16.43
ΔE_{SURF}	40.87	0.84	40.68	0.82	10.96	0.19	-10.76	0.38
ΔG_{gas}	-8192.00	34.49	-6608.75	31.12	-1080.85	16.19	-502.41	18.49
ΔG_{solv}	-1136.88	24.19	-1203.41	22.76	-379.52	12.82	446.06	16.19
ΔG_{TOTAL}	-9328.88	26.38	-7812.16	23.31	-1460.37	7.37	**-56.35**	4.64
TS_{TRA}	16.06	0.00	15.93	0.00	14.29	0.00	-14.16	0.00
TS_{ROT}	15.93	0.00	15.76	0.00	13.17	0.01	-13.01	0.01
TS_{VIB}	1138.95	2.35	973.43	2.87	141.41	1.16	24.11	3.65
TS_{TOT}	1170.94	2.36	1005.12	2.87	168.87	1.16	**-3.06**	3.66
$\Delta G_{binding}$							**-53.29**	

Electrostatic energy (**ΔE_{EL}**); van der Waals contribution (**$\Delta E_{VDWAALS}$**); total gas phase energy (**ΔG_{gas}**); nonpolar contribution to the solvation free energy (**ΔE_{SURF}**); the electrostatic contribution to the solvation free energy (**ΔE_{GB}**); sum of nonpolar and polar

contributions to solvation (ΔG_{solv}); final estimated binding free energy (ΔG_{TOTAL}); translational energy (TS_{TRA}); rotational energy (TS_{ROT}); vibrational energy (TS_{VIB}), total entropic contribution (TS_{TOT}); binding free energy ($\Delta G_{binding}$).

Table 4.4. *The various components of the BFE (kcal mol^{-1}) evaluated by MM/PBSA method between p53-MDM2 complex.*

	p53-MDM2		MDM2		p53		Delta	
	Average	Std. Dev. (±)	Average	Std. Dev. (±)	Average	Std. Dev. (±)	Average	Std. Dev. (±)
$\Delta E_{VDWAALS}$	-776.69	12.17	-638.49	11.02	-65.47	3.10	-72.72	5.38
ΔE_{EL}	-7415.31	32.88	-5970.25	31.26	-1015.38	16.09	-429.68	16.07
ΔE_{PB}	-1153.54	21.57	-1191.66	20.58	-410.03	12.71	448.15	16.30
ΔE_{NPOLAR}	849.68	3.88	761.05	3.86	146.79	1.26	-58.16	1.99
ΔE_{DISPER}	-520.70	3.46	-496.58	3.93	-126.18	0.98	102.06	2.38
ΔG_{gas}	-8192.00	34.49	-6608.75	31.12	-1080.85	16.19	-502.41	18.49
ΔG_{solv}	-824.56	19.95	-927.20	19.43	-389.42	12.80	492.06	16.79
ΔG_{TOTAL}	-9016.56	27.48	-7535.94	24.79	-1470.27	7.71	**-10.35**	4.91
TS_{TRA}	16.06	0.00	15.93	0.00	14.29	0.00	-14.16	0.00
TS_{ROT}	15.93	0.00	15.76	0.00	13.17	0.01	-13.01	0.01
TS_{VIB}	1138.95	2.35	973.43	2.87	141.41	1.16	24.11	3.65
TS_{TOT}	1170.94	2.36	1005.12	2.87	168.87	1.16	**-3.06**	3.66
$\Delta G_{binding}$							**-7.29**	

Electrostatic energy (ΔE_{EL}); van der Waals contribution ($\Delta E_{VDWAALS}$); total gas phase energy (ΔG_{gas}); nonpolar contribution to the solvation free energy ($\Delta E_{NPOLAR} + \Delta E_{DISPER}$); the electrostatic contribution to the solvation free energy (ΔE_{PB}); sum of nonpolar and polar contributions to solvation (ΔG_{solv}); final estimated binding free energy (ΔG_{TOTAL}); translational energy (TS_{TRA}); rotational energy (TS_{ROT}); vibrational energy (TS_{VIB}), total entropic contribution (TS_{TOT}); binding free energy ($\Delta G_{binding}$).

From **Table 4.3** and **4.4**, we observed that all the derived components for the BFE analysis contributed to the binding of p53 and MDM2 to form the p53-MDM2 complex. The $\Delta G_{binding}$ for the p53-MDM2 complex was calculated to be -53.29 kcal mol^{-1} and -7.29 kcal mol^{-1} using MM-GBSA and MM-PBSA methods respectively. We found the

calculated BFE value for the p53-MDM2 complex using MM-PBSA to be more closer to the experimental values (-6.4 to -9.0 kcal mol^{-1}). To ensure the BFE findings, we have carried out the duplicate simulation run and also another simulation using different force field (ff99SB-ILDN) for the p53-MDM2 complex. The BFE results obtained for the duplicate simulation run and for the simulation with ff99SB-ILDN force field have been summarized in the **Tables 4.5**, **4.6**, **4.7** and **4.8**. From these tables, we observe the BFE values calculated using MM-PBSA method to be closer to the experimental values.

Table 4.5. *The various components of the BFE (kcal mol^{-1}) evaluated by MM/GBSA method between p53-MDM2 complex for duplicate simulation run.*

	p53-MDM2		MDM2		p53		Delta	
	Average	Std. Dev. (±)	Average	Std. Dev. (±)	Average	Std. Dev. (±)	Average	Std. Dev. (±)
$\Delta E_{VDWAALS}$	-769.84	12.48	-634.98	9.63	-62.16	3.49	-72.70	4.26
ΔE_{EL}	-7392.50	33.30	-5969.48	30.65	-1025.39	19.29	-397.62	13.21
ΔE_{GB}	-1282.03	24.67	-1284.64	22.64	-420.79	11.68	423.41	9.62
ΔE_{SURF}	44.07	0.75	42.90	0.64	11.81	0.14	-10.64	0.40
ΔG_{gas}	-8162.33	32.71	-6604.46	31.08	-1087.55	18.55	-470.32	12.21
ΔG_{solv}	-1237.97	24.42	-1241.74	22.40	-408.99	11.68	412.76	9.58
ΔG_{TOTAL}	-9400.30	20.70	-7846.20	19.32	-1496.54	9.61	**-57.55**	4.76
TS_{TRA}	16.06	0.00	15.93	0.00	14.29	0.00	-14.16	0.00
TS_{ROT}	15.93	0.00	15.76	0.01	13.21	0.01	-13.04	0.01
TS_{VIB}	1147.21	3.21	975.18	3.26	146.85	0.79	25.18	1.92
TS_{TOT}	1179.20	3.21	1006.80	3.26	174.35	0.79	**-2.02**	1.93
$\Delta G_{binding}$							**-55.53**	

Electrostatic energy (ΔE_{EL}); van der Waals contribution ($\Delta E_{VDWAALS}$); total gas phase energy (ΔG_{gas}); nonpolar contribution to the solvation free energy (ΔE_{SURF}); the electrostatic contribution to the solvation free energy (ΔE_{GB}); sum of nonpolar and polar contributions to solvation (ΔG_{solv}); final estimated binding free energy (ΔG_{TOTAL}); translational energy (TS_{TRA}); rotational energy (TS_{ROT}); vibrational energy (TS_{VIB}), total entropic contribution (TS_{TOT}); binding free energy ($\Delta G_{binding}$).

Table 4.6. *The various components of the BFE (kcal mol^{-1}) evaluated by MM/PBSA method between p53-MDM2 complex for duplicate simulation run.*

	p53-MDM2		MDM2		p53		Delta	
	Average	Std. Dev. (±)	Average	Std. Dev. (±)	Average	Std. Dev. (±)	Average	Std. Dev. (±)
$\Delta E_{VDWAALS}$	-769.84	12.48	-634.96	9.63	-62.16	3.49	-72.70	4.26

ΔE_{EL}	-7392.50	33.30	-5969.48	30.65	-1025.39	19.29	-397.62	13.21
ΔE_{PB}	-1252.89	25.42	-1231.91	22.48	-437.82	10.91	416.84	9.55
ΔE_{NPOLAR}	865.05	4.09	770.76	3.58	151.43	1.02	-57.14	1.78
ΔE_{DISPER}	-536.13	3.84	-505.02	3.65	-130.66	0.86	99.55	2.20
ΔG_{gas}	-8162.33	32.71	-6604.46	31.08	-1087.55	18.55	-470.32	12.21
ΔG_{solv}	-923.97	24.89	-966.17	22.01	-417.05	10.83	459.26	9.47
ΔG_{TOTAL}	-9086.30	22.31	-7570.63	21.42	-1504.61	11.77	**-11.06**	7.04
TS_{TRA}	16.06	0.00	15.93	0.00	14.29	0.00	-14.16	0.00
TS_{ROT}	15.93	0.00	15.76	0.01	13.21	0.01	-13.04	0.01
TS_{VIB}	1147.21	3.21	975.18	3.26	146.85	0.79	25.18	1.92
TS_{TOT}	1179.20	3.21	1006.80	3.26	174.35	0.79	**-2.02**	1.93
$\Delta G_{binding}$							**-9.04**	

Electrostatic energy (ΔE_{EL}); van der Waals contribution ($\Delta E_{VDWAALS}$); total gas phase energy (ΔG_{gas}); nonpolar contribution to the solvation free energy ($\Delta E_{NPOLAR} + \Delta E_{DISPER}$); the electrostatic contribution to the solvation free energy (ΔE_{PB}); sum of nonpolar and polar contributions to solvation (ΔG_{solv}); final estimated binding free energy (ΔG_{TOTAL}); translational energy (TS_{TRA}); rotational energy (TS_{ROT}); vibrational energy (TS_{VIB}), total entropic contribution (TS_{TOT}); binding free energy ($\Delta G_{binding}$).

Table 4.7. *The various components of the BFE (kcal mol^{-1}) evaluated by MM/GBSA method between p53-MDM2 complex using force field ff99SB-ILDN.*

	p53-MDM2		MDM2		p53		Delta	
	Average	Std. Dev. (±)	Average	Std. Dev. (±)	Average	Std. Dev. (±)	Average	Std. Dev. (±)
$\Delta E_{VDWAALS}$	-777.21	11.38	-640.45	9.31	-62.18	3.71	-74.58	2.98
ΔE_{EL}	-7309.45	33.13	-5919.86	26.65	-1032.21	15.08	-357.38	20.28
ΔE_{GB}	-1331.60	25.86	-1304.63	19.39	-414.75	11.74	387.78	19.01
ΔE_{SURF}	43.16	0.72	41.78	0.61	11.22	0.22	-9.84	0.28
ΔG_{gas}	-8086.66	32.70	-6560.31	27.87	-1094.39	15.50	-431.96	20.37
ΔG_{solv}	-1288.44	25.69	-1262.85	19.18	-403.53	11.58	377.94	18.93
ΔG_{TOTAL}	-9375.10	23.43	-7823.16	19.94	-1497.92	7.66	**-54.02**	3.95
TS_{TRA}	16.06	0.00	15.93	0.00	14.29	0.00	-14.16	0.00
TS_{ROT}	15.93	0.00	15.77	0.00	13.18	0.01	-13.02	0.01
TS_{VIB}	1147.86	2.71	980.94	2.26	140.82	0.55	26.10	3.47
TS_{TOT}	1179.84	2.72	1012.63	2.26	168.29	0.56	**-1.09**	3.47
$\Delta G_{binding}$							**-52.93**	

Electrostatic energy (ΔE_{EL}); van der Waals contribution ($\Delta E_{VDWAALS}$); total gas phase energy (ΔG_{gas}); nonpolar contribution to the solvation free energy (ΔE_{SURF}); the electrostatic contribution to the solvation free energy (ΔE_{GB}); sum of nonpolar and polar contributions to solvation (ΔG_{solv}); final estimated binding free energy (ΔG_{TOTAL}); translational energy (TS_{TRA}); rotational energy (TS_{ROT}); vibrational energy (TS_{VIB}), total entropic contribution (TS_{TOT}); binding free energy ($\Delta G_{binding}$).

Table 4.8. *The various components of the BFE (kcal mol^{-1}) evaluated by MM/PBSA method between p53-MDM2 complex using force field ff99SB-ILDN.*

	p53-MDM2		MDM2		p53		Delta	
	Average	Std. Dev. (±)	Average	Std. Dev. (±)	Average	Std. Dev. (±)	Average	Std. Dev. (±)
$\Delta E_{VDWAALS}$	-777.21	11.38	-640.45	9.31	-62.18	3.71	-74.58	2.98
ΔE_{EL}	-7309.45	33.13	-5919.86	26.65	-1032.21	15.08	-357.38	20.28
ΔE_{PB}	-1310.25	26.39	-1262.99	20.97	-427.03	11.75	379.77	19.92
ΔE_{NPOLAR}	858.75	4.18	763.94	3.88	150.07	1.36	-55.26	1.42
ΔE_{DISPER}	-531.67	3.85	-501.31	3.29	-129.24	1.27	98.88	1.60
ΔG_{gas}	-8086.66	32.70	-6560.31	27.87	-1094.39	15.50	-431.96	20.37
ΔG_{solv}	-983.17	26.53	-1000.36	20.75	-406.20	11.74	423.39	20.55
ΔG_{TOTAL}	-9069.83	23.68	-7560.67	21.01	-1500.59	7.36	**-8.57**	4.94
TS_{TRA}	16.06	0.00	15.93	0.00	14.29	0.00	-14.16	0.00
TS_{ROT}	15.93	0.00	15.77	0.00	13.18	0.01	-13.02	0.01
TS_{VIB}	1147.86	2.71	980.94	2.26	140.82	0.55	26.10	3.47
TS_{TOT}	1179.84	2.72	1012.63	2.26	168.29	0.56	**-1.09**	3.47
$\Delta G_{binding}$							**-7.48**	

Electrostatic energy (ΔE_{EL}); van der Waals contribution ($\Delta E_{VDWAALS}$); total gas phase energy (ΔG_{gas}); nonpolar contribution to the solvation free energy ($\Delta E_{NPOLAR} + \Delta E_{DISPER}$); the electrostatic contribution to the solvation free energy (ΔE_{PB}); sum of nonpolar and polar contributions to solvation (ΔG_{solv}); final estimated binding free energy (ΔG_{TOTAL}); translational energy (TS_{TRA}); rotational energy (TS_{ROT}); vibrational energy (TS_{VIB}), total entropic contribution (TS_{TOT}); binding free energy ($\Delta G_{binding}$).

To know the contribution of the interacting amino acid residues at the interface to the overall PPI of the p53-MDM2 complex, PRED values were calculated using the MM-PBSA module of the AMBER 14 software package [584-586]. The PRED results for the entire interface residues present in our complex have been given in **Figure 4.12**. The highest energy contributions for MDM2 come from the residues LYS51, LEU54, TYR100, and TYR104. On the other hand, the highest energy contributions for p53 come from the residues PHE19, TRP23, and LEU26.

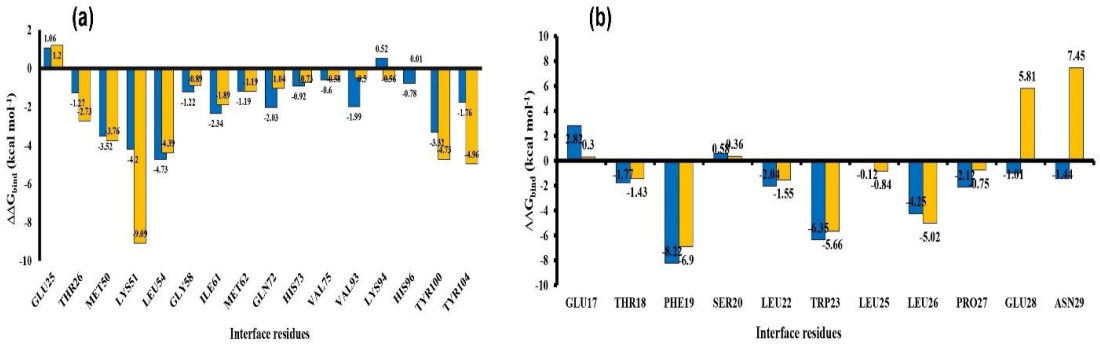

Figure 4.12. *Per Residue Energy Decomposition (PRED) plots for the interface residues of (a) MDM2 and (b) p53.*

4.5. Conclusion:

In this work, we have demonstrated the binding and unbinding mechanisms of the p53(TAD1)-MDM2(NTD) complex by calculating PMF using US simulations. The p53-MDM2 complex structure with minimum PMF value was obtained at a CoM distance of separation of 12 Å, with a dissociation energy of 30 kcal mol^{-1}. The distance of separation of p53 from MDM2 was found to affect the secondary structure content (helical and turns) and the stability of the p53 molecule. We have also monitored the different folding patterns of p53 during the course of its separation from MDM2. These folding pattern inferences are very much important to design the methods of inhibition for p53-MDM2 complex. We also found hydrogen bonds and salt bridge between Lys94 of MDM2 and Glu17 of p53 to be critical factors for the stability of the p53-MDM2 complex. The binding affinity between MDM2 and p53 was observed to be indeed high (ΔG_{bind} = -7.29 kcal mol^{-1} from MM-PBSA and ΔG_{bind} = -53.29 kcal mol^{-1} from MM-GBSA). The binding energy calculated for the p53-MDM2 complex using MM-PBSA method was found to be near to the experimental binding values. The binding energy values for the complex estimated using MM-PBSA and MM-GBSA methods were ensured by performing the duplicate simulation run and also simulation with another force field. From the PRED analysis, the residues Lys51, Leu54, Tyr100, and Tyr104 from MDM2 and the residues Phe19, Trp23, and Leu26 from p53 were found to provide the highest energy contributions for the p53-MDM2 interaction. Our findings in this study provide insights into the binding pathway and the degree of association of p53 and MDM2 in forming the complex. These findings may be useful for designing potential inhibitors that disrupt the p53-MDM2 interactions.